Physics of the Earth and Planetary Interiors 176 (2009) 109–123

Contents lists available at ScienceDirect

Physics of the Earth and Planetary Interiors

journal homepage: www.elsevier.com/locate/pepi

Paleomagnetism of the Fentale-magmatic segment, main Ethiopian Rift: New evidence for counterclockwise block rotation linked to transtensional deformation

Tesfaye Kidane[a,b,*], Yo-Ichiro Otofuji[b], Yutaka Komatsu[b], Hisaya Shibasaki[b], Julie Rowland[c]

[a] Department of Earth Sciences, Faculty of Science, Addis Ababa University, P.O. Box 1176, Addis Ababa, Ethiopia
[b] Department of Earth and Planetary Sciences, Science Faculty, Kobe University, Kobe 657-8501, Japan
[c] School of Geography, Geology, and Environmental Sciences, University of Auckland, New Zealand

ARTICLE INFO

Article history:
Received 9 January 2009
Received in revised form 18 March 2009
Accepted 16 April 2009

Keywords:
Paleomagnetism applied to tectonics
Main Ethiopian Rift
Fentale volcanoes
Transtension
Block rotation

ABSTRACT

We carried out the first ever paleomagnetic investigations in the area around the Fentale volcanoes, Main Ethiopian Rift. A total of 28 paleomagnetic sites were sampled around the two Fentale (Tinish and Tilik) volcanic centers. Lava and pyroclastic flows ranging in age from 2 Ma to 0.1 Ma was sampled for this study. After routine paleomagnetic collection and sample preparation procedures specimens were subjected to progressive alternating fields and thermal demagnetizations. The directional analysis shows either one or two components of Natural Remanent Magnetization to characterize the entire measurements. The low stability components are removed either by alternating fields up to 15 mT or by heating up to 250 °C. The high stability and primary components are isolated above those steps and vector is directed towards the origin, and it represents the Characteristic Remanent Magnetization. The principal component analysis and site means directions calculations yielded normal and reversed polarities together with two anomalous directions. When an overall mean direction is calculated from the individual site mean directions for the Fentale region, $D_s = 354.3°$, $I_s = 19.3°$, $N = 27$, $K = 33$, $\alpha_{95} = 4.9°$ are obtained. When this result is compared with the mean expected reference dipole geomagnetic field direction ($D = 1.0°$, $I = 16.4°$, $\alpha_{95} = 2.3°$, $K = 105.6$, $N = 32$) for an average age of 1.5 Ma, the following differences of $\Delta D = -6.7° \pm 4.3°$, $\Delta I = -2.9° \pm 4.3°$ can be obtained. These results from the region indicate ~7° counterclockwise block rotations about vertical axis consistent with the transtentional deformations that characterize the Fentale magmatic segment.

1. Introduction

The Ethiopian Rift valley is part of the East African Rift System and it stretches from Lake Abaya in the south to the Gabilema volcano in the north (Fig. 1). The Main Ethiopian Rift (MER) is the 700 km long, 80 km wide volcanically active rift situated between the northwestern and southeastern Ethiopian Plateaus. Along the flanks of the rift, large offset border faults are characterized by rift-ward *en échelon* right-stepping normal faults with a dominant orientation of NNE-SSW & NE-SW directions and distinctive structural styles (Fig. 2) (Di Paola, 1972; Casey et al., 2006). The eastern margin fault systems are defined by multiple faults with cumulative displacement greater than 100 m on each of the contributing faults, whereas; the western margin is marked by a long escarpment with an exposed throw of 1.5 km (e.g. Woldegabriel et al., 1990; Abebe, 1993). Between these border faults, the central rift valley is marked by approximately 20 km-wide, right-stepping, en echelon chains of eruptive volcanic centers, extension cracks, fissures and N15E striking, small offset normal faults (e.g. Boccaletti et al., 1998, Ebinger and Casey, 2001 and Abebe, 1993). These right stepping *en échelon* faults, fissures and chains of Quaternary eruptive centers were collectively referred to as the Wonji Fault Belt (WFB), which Mohr (1962) and Meyer et al. (1975) interpreted as a rift-ward migration of strain from border faults. With better geochronology data and imagery, Ebinger and Casey (2001) delineated Quaternary along-axis segmentation of faults and eruptive centers, and described a series of magmatic segments within the loosely defined WFB. The along-axis segmentation of the WFB is apparent down to mid-lower crustal levels: high-velocity, high-density material, interpreted as cooled mafic intrusion, rises to about 8 km depth beneath the 50 km-long 'magmatic segments' (Mahatsente et al., 1999; Keranen et al., 2004).

* Corresponding author at: Department of Earth Sciences, Faculty of Science, Addis Ababa University, P.O. Box 1176, Addis Ababa, Ethiopia.
E-mail address: tesfkida@geol.aau.edu.et (T. Kidane).

0031-9201/$ – see front matter © 2009 Elsevier B.V. All rights reserved.
doi:10.1016/j.pepi.2009.04.006

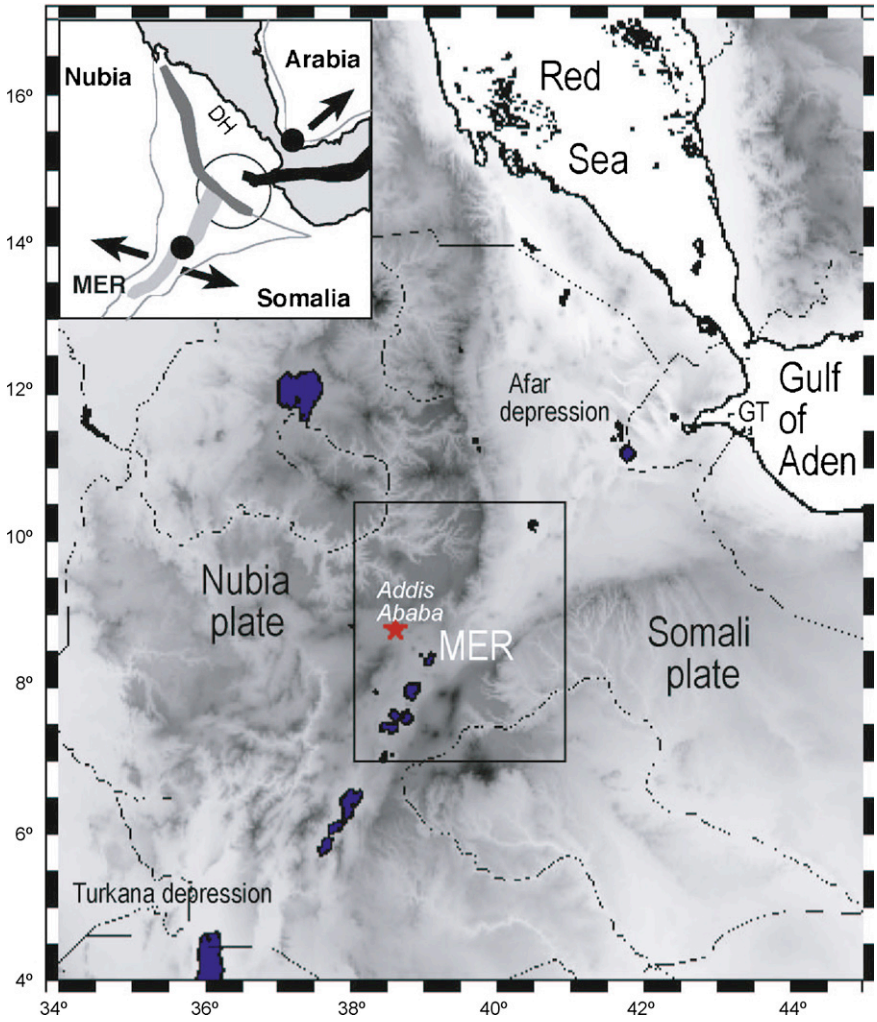

Fig. 1. Digital Elevation Map of the Main Ethiopian Rift (MER) with the bordering plateaus. The Fentale magmatic segment is with in the rectangle.

Based on interpretation of geological and geophysical data, Ebinger and Casey (2001) identified five 'magmatic segments (MS)', which they likened to the along-axis segmentation observed on slow spreading mid-oceanic ridges. These magmatic segments, named after the peralkaline silicic volcanic centers present in each segment, are Aluto-Gedemsa, Boset-Kone, Fentale-Dofen, Angelele, and Addo-do MS, respectively from south to north. The average elevation of each segment decreases from south to north. The Aluto-Gedemsa segment (not caldera peak) lies at an altitude of 1900 m above sea level, the Boset-Kone segment is ~500 m lower and the Fentale-Dofen segment, which occupies a half graben, averages <850 m above sea level. The positive relief of the Aluto-Gedemsa and Boset-Kone MS deflect rivers away, whereas the shallow depressions of the Fentale-Dofen and Angelele MS capture the Awash River and its tributaries. Crustal thickness also decreases from 38 km beneath Aluto-Gedemsa to 26 km under Fentale-Dofen segments consistent with the variation in elevation (e.g. Casey et al., 2006).

2. Tectonic and geologic setting

The Main Ethiopian Rift system developed within an Oligocene flood basalt province, and it overlies a broad region of anomalously low velocity mantle (e.g. Benoit et al., 2003; Bastow et al., 2005). A synthesis of $^{40}Ar/^{39}Ar$ data shows that a 1–2 km thickness of mainly flood basalts erupted to form the Ethiopian and Yemen plateaus between 31–30 Ma or 29 Ma (e.g. Hofmann et al., 1997; Pik et al., 2003). The main outpouring of the Ethio-Yemen trap series is linked genetically to the Afro-Arabian continental breakup. However, some volcanism persisted and extended over large areas outside the developing rifts until ~11 Ma (e.g. Kieffer et al., 2004; Wolfenden et al., 2005), when the bulk of volcanism was localized within the developing rift valley. Less voluminous volcanic products of that age extend several hundred kilometers further to the north (e.g. Kenea et al., 2001). An earlier probably related volcanic phase between 45–39 Ma affected southwest Ethiopia (e.g. Ebinger et al., 2000), though evidence of earlier faulting is nonexistent.

The kinematic evolution of the rift and the along-axis segmentation of the WFB have been interpreted in various ways. Di Paola (1972) and Woldegabriel et al. (1990) invoke an E-W extension direction during the entire rift evolution. In contrast, a consistent NW-SE extension has also been proposed (Chorowicz et al., 1994; Korme et al., 1997; Acoccella and Korme, 2002). Recent structural investigations in the Assela and Nazreth area are consistent with a change in extension direction from NW-SE to E-W during the Quaternary with implications for vertical axis block rotations (Boccaletti et al., 1994; Abebe, 1993; Bonini et al., 1997). However, paleomagnetic results from the same region indicated an absence of vertical axis rotations (Kidane et al., 2006).

The structural grain of the MER, including the orientation of the border faults, shows significant along-strike variations. In the south,

the orientation of the border faults is N-S, in the Assela area the orientation changes to NE-SW, and further north, the eastern margin has an E-W in orientation while the western margin is oriented N-S. The orientation of the rift axis faults (WFB) themselves show orientation changes along strike as well. The above parameters show variations along strike going south to north from Boset-Kone to Fentale-Dofen and Angelele MS. The rift axis is also dextrally offset with variable width and overlap length (Fig. 2). The density of faulting and the length of faults and fissures change as one goes from the southern segment to the northern (Casey et al., 2006).

The Fentale region is one of several magmatic-tectonic segments in the main Ethiopian Rift. Crustal thickness decreases from about 38 km close to Assela area to about 26 km in this magmatic segment. There is a significant drop in altitude from the Assela-Munessa area with in the Aluto-Gedemsa magmatic segment to the Fentale segment. The width of the rift valley itself widens from about 70 km near the Assela Munessa to more than 100 km near the Fentale area. Previous paleomagnetic work in the Assela area showed no rotation that could be seen in paleomagnetism where as previous model (Boccaletti et al., 1992) predicted counterclockwise rotations linked to oblique rifting for the entire main Ethiopian Rift.

Around the Fentale region, the width of the rift dramatically increases and faults of multiple orientations forming rhomb-shaped basins are observed. Based on the geometries of the faults in this particular magmatic segment, Casey et al. (2006) suggested these fault patterns as indicative of transtensional kinematics.

The above first order observations demonstrate that the structural grain at border fault and intra-rift scale varies along the strike of the MER. Moreover, results from geophysical and structural investigations (Ebinger and Casey, 2001; Casey et al., 2006; Kidane et al., 2006) support a notion that the MER may have undergone differential kinematics with consequent temporal and spatial variations in deformation style. However, proposed kinematic models for the MER do not account adequately for these structural variations and are often in conflict (Boccaletti et al., 1998). This situation arises partly because macroscopic studies (10^0–10^2 km in scale) have been scaled-up to explain the kinematics of the entire MER. Systematic rift-wide investigations are required to develop models for each region within the MER, thereby allowing development of a comprehensive mechanical model that could explain most geological and geophysical observations.

In this paper, we report the results of paleomagnetic investigations undertaken around the Fentale-Dofen MS, thereby expanding our earlier contribution which focused on the northern sector of the Aluto-Gedemsa MS. Along strike variability in geological and geophysical observations of the MER is the main scientific rational behind our current undertaking. We target the volcanic products of the Tinish and Tilik Fentale volcanic edifices, which broadly include lava and pyroclastic flows.

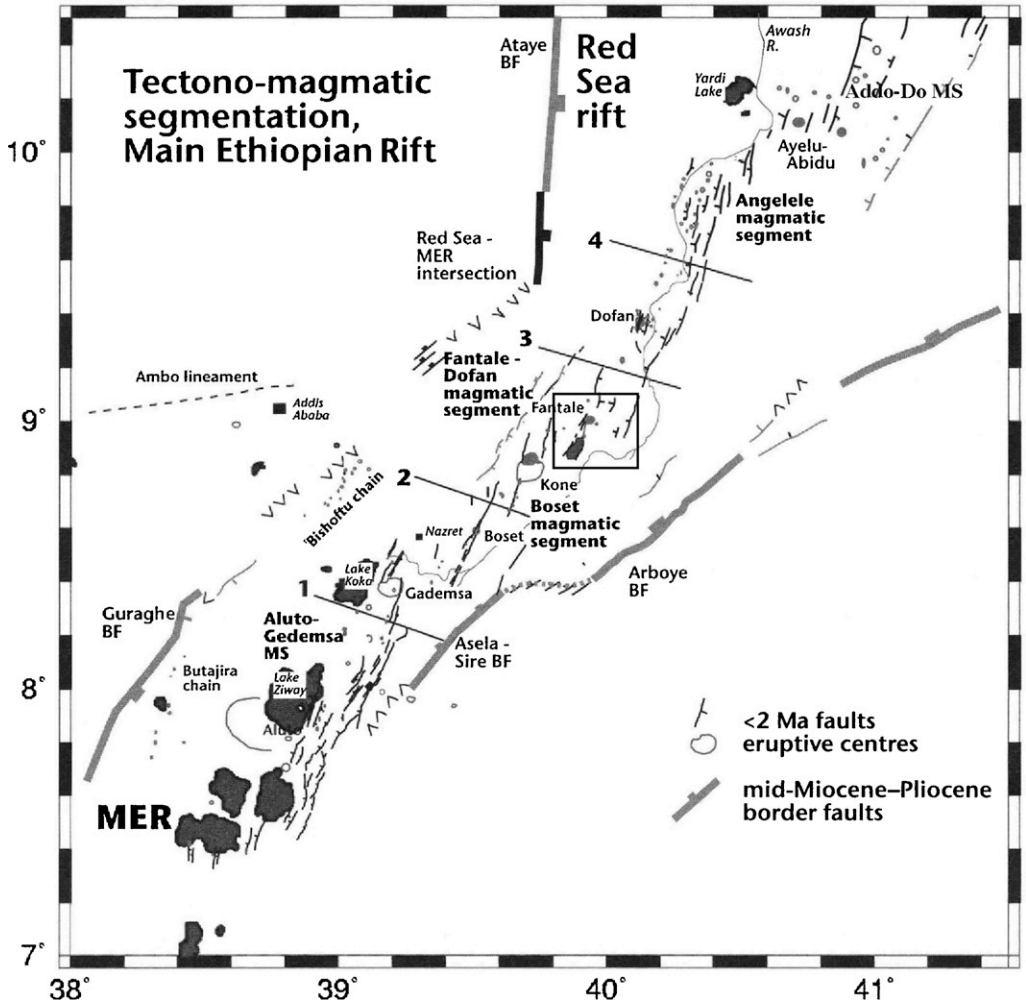

Fig. 2. (a) Tectonic map (of the Main Ethiopian Rift showing the major structural grain and magmatic segments. The Fentale area is indicated with small rectangle (from Casey et al., 2006). (b) Geological map of the study area showing the major lithologies that were sampled (modified from Williams et al., 2004), on which the distributions of the paleomagnetic sites are indicated.

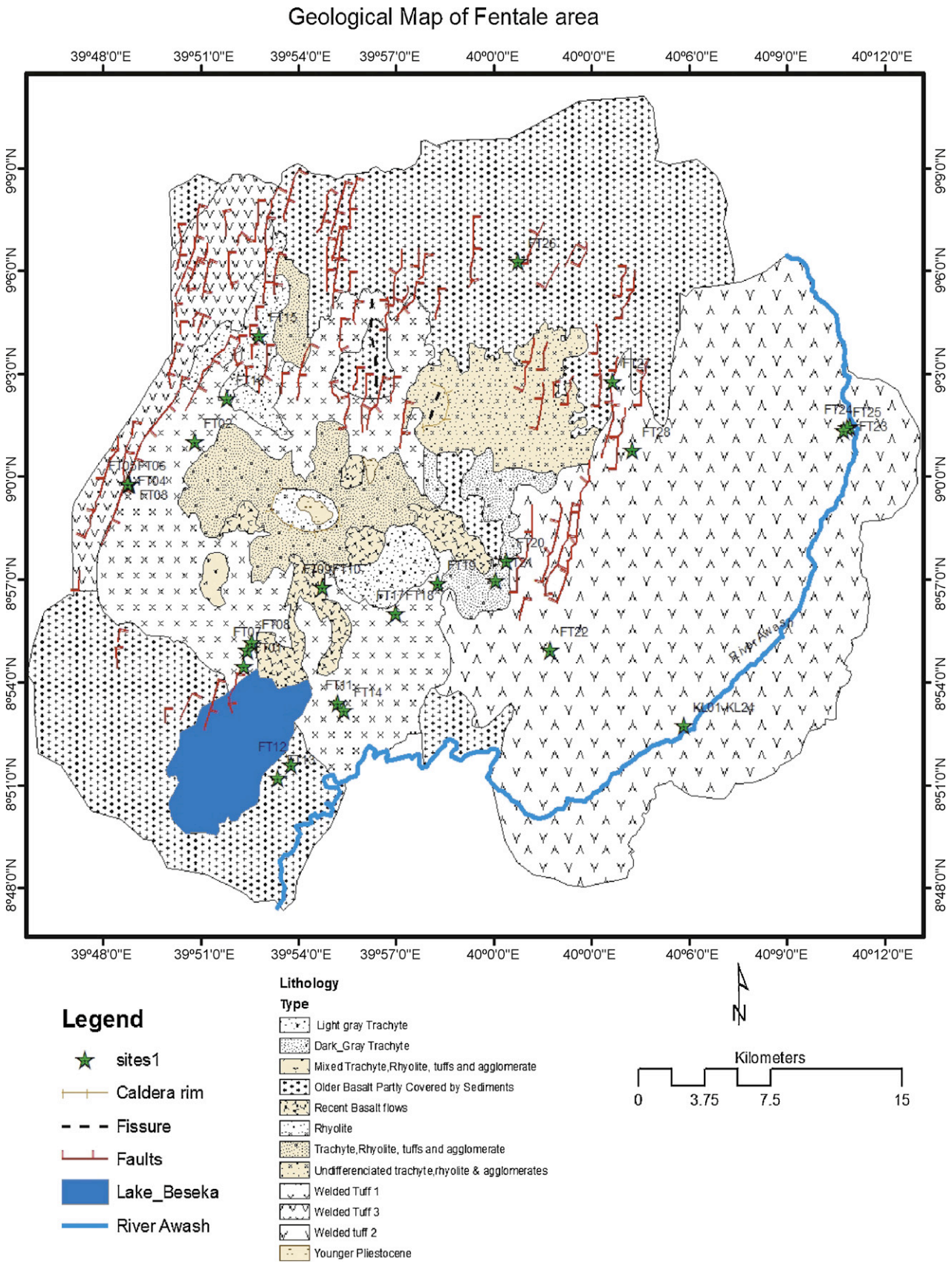

Fig. 2. (*Continued*).

Tilik Volcano is the main Fentale volcanic edifice and it is the major central volcano in this magmatic segment. The volcano rises some 600 m from the floor of the rift and the volcanic products around it are outpoured either from itself or the other smaller center (Tinish Fentale), which lies close to the pre-collapse summit of the volcano. The rocks that outcrop consist of lava flows, particularly basalts, trachytes and rhyolites, and pyroclastic flows particularly ignimbrites and welded tuffs, which from previous investigations (except rhyolite) are known to be very suitable for paleomagnetic investigations (Acton et al., 2000; Kidane et al., 2006). Existing radio-isotopic data indicate that the ages of the rocks analyzed range between 1.9 and 0.2 Ma; an older trachyte unit has been dated, using K/Ar dating (Williams et al., 2004) at 1.86 ± 0.1 Ma. The oldest welded tuff (ignimbrite) from Tinish Fentale is dated at 1.51 Ma (K/Ar, Williams et al., 2004) along the section in the Awash Gorge. The welded tuff from main Fentale volcano is dated at 0.17 ± 0.04 Ma (Williams et al., 2004).

3. Paleomagnetism

Paleomagnetic investigations are limited throughout the main Ethiopian rift: Kidane et al. (2006) made the first such study, which was focused in the regions around Assela and Nazreth, though it included a single site from the current study area.

3.1. Field and laboratory procedure

The rock types we collected for paleomagnetism study include mafic, and intermediate lava flows; basalts, and trachytes and pyroclastic flows mainly ignimbrite. Fresh and unaltered exposures were obtained mostly along fault scarps, river valleys and quarry cuts. Very young pitchstone and rhyolites outcropping along the flanks and inside of the caldera have systematically been avoided for their bad demagnetization behavior, and have not been sampled. We carefully selected rock units (sites) such as basalts, trachytes, and ignimbrites with age intervals of only between 2.02 ± 0.12 Ma and 0.17 Ma for our paleomagnetic study. The youngest rock units, historical lava flows, pitchstones, and rhyolites, which are generally younger than 0.17 Ma, were not sampled because of their age and also because the rhyolites have a poor record for behaving well upon demagnetization (Kidane et al., 2003). We collected samples from 28 sites spatially distributed around the Fentale volcano and 24 more sites along the Kereyu Lodge Awash River section in the Awash National Park. The distribution of these sites is shown in Fig. 2b. A Japanese and Ethiopian team composed of 4 scientists participated in the sampling in February 2006. The sampling was done using the standard Pomeroy, gasoline-powered portable drill and NATSUHARA modified Pomeroy drilling apparatus. At least 10 cylindrical core samples with an average 10 cm length were collected from each paleomagnetic site. Core samples were oriented on site using the standard orienting fixtures; relevant information was marked on the samples, which were identified from FT01 to FT 28 (FT-stands for Fentale) for the spatial sampling; and from KL01 to KL24 (KL stands for Kereyou Lodge) for the temporal samples along the Kereyu Lodge Magnetostratigraphy section. The detailed work along the Kereyou Lodge section is presented as a magnetostratigraphy report in a companion paper (GJI under review) but relevant directional data from that study are included here particularly for the purpose of obtaining an overall mean direction for the Metehara region. Mostly magnetic compass orientations were taken because of persistent shadows during the sampling season and partly because we had relied on the prior detailed paleomagnetic surveys, which demonstrated that the difference between the magnetic and sun compasses averaged to zero and that local anomalies due to the lightening strikes are not significant (Kidane et al., 1999, 2003, 2006).

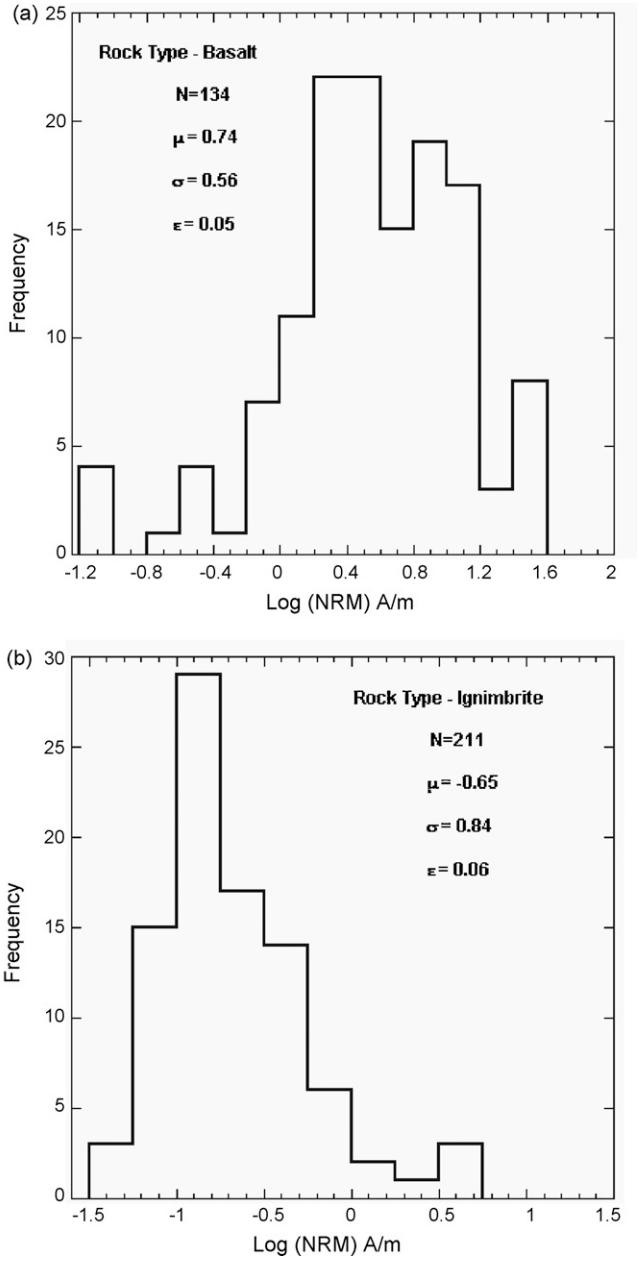

Fig. 3. Histogram of the natural remanent magnetization intensity (NRM) for the two major rock types (a) basalt and (b) ignimbrite.

The oriented core samples were cut to standard 2.2 cm twin specimens. One specimen from all core samples was subjected to progressive alternating field (AF), and the other was subjected to progressive heating (TH) treatment techniques in order to confirm the directions obtained from the two techniques. All paleomagnetic measurements and analyses of the samples were treated in the state of the art paleomagnetism laboratory facility at the Department of Earth and Planetary Sciences of Kobe University. AF demagnetization was carried out using the Natsuhara DEM-8601 AF demagnetizing equipment and Thermal demagnetization was made using the Natsuhara TDS-1 thermal demagnetizer. Magnetization measurements were done on the vertical access Squid magnetometer and Molspin spinner magnetometer. Data obtained

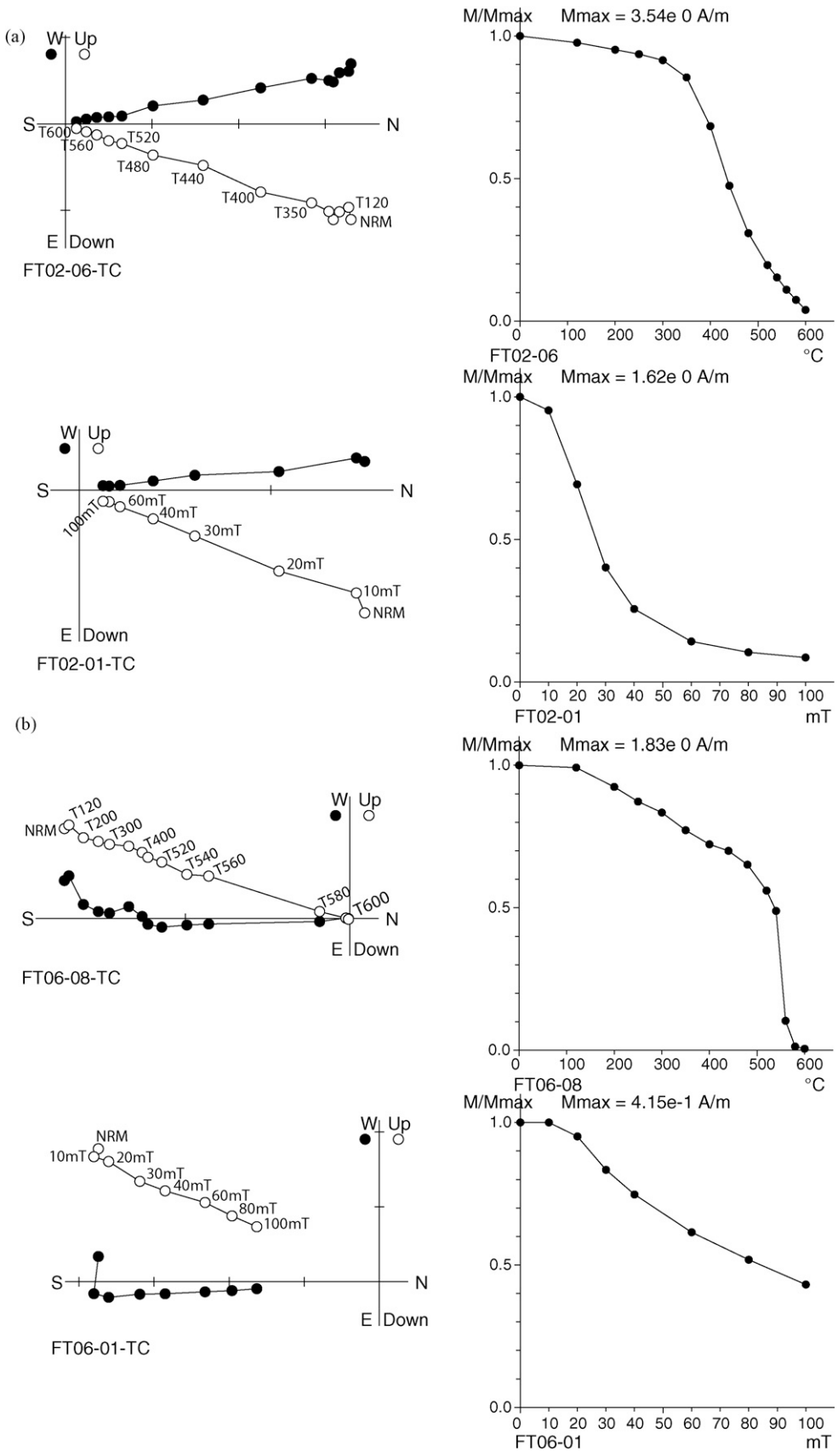

Fig. 4. Representative vector component diagrams representing the characteristics behavior of the NRM directions samples for the samples analyzed. (a) The first two specimens are from basalt while the next two (b) are from ignimbrite units. The former represent examples for normal polarity while the latter examples for reversed polarity. (c) Examples of vector component diagrams for trachyte samples analyzed; in all the three examples, top specimen was treated by thermal while bottom specimen by alternating field demagnetization techniques respectively; the two techniques gave identical results with quasi-single component. Solid circles are the component in the horizontal (N-S versus W-E) plane; open circles are the component in the N-S vertical plane.

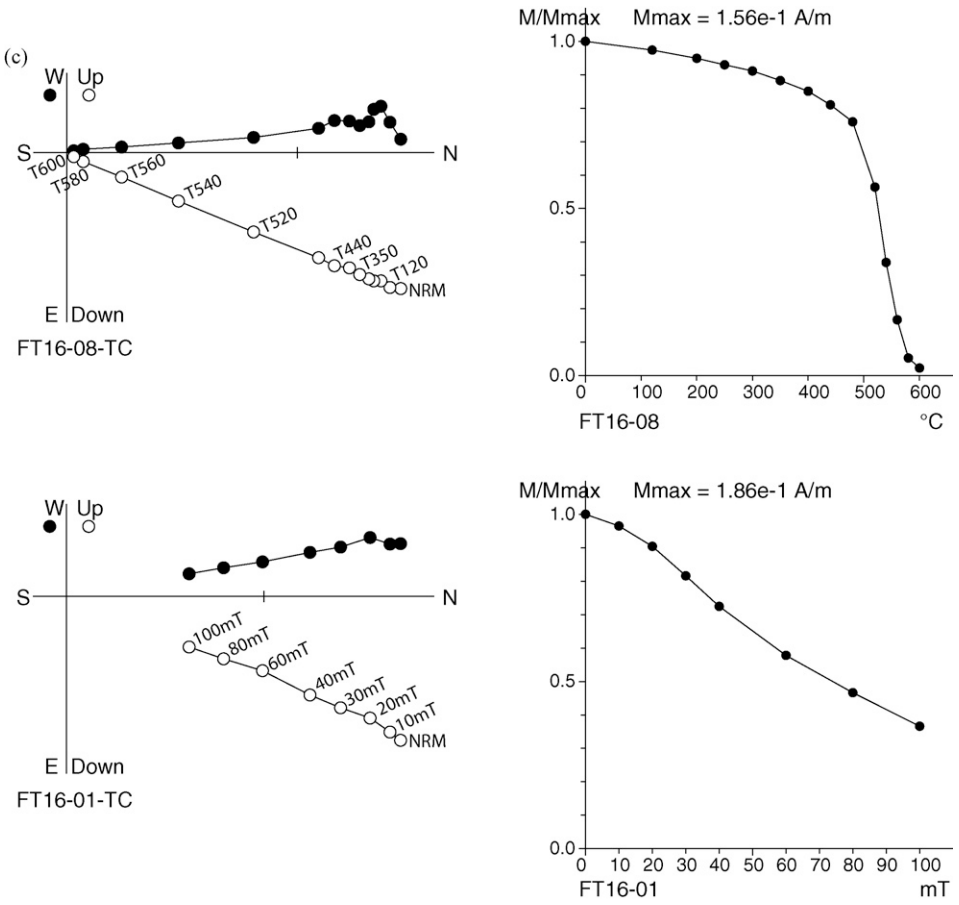

Fig. 4. (*Continued*).

from the Squid was transferred into the Paleomac format and analyzed using the Paleomac software package (Cogné, 2003).

3.2. Natural remanent magnetization (NRM)

Both types of rocks, lavas and pyroclastic flows, have high Natural Remanent Magnetization (NRM) intensities and the paleomagnetic directions they recorded were excellent. The NRM of both the basalt and ignimbrite in Fentale area are plotted in separate histograms by lithology. Fig. 3 shows the histograms for the analyzed speciments from 134 basalts and 211 ignimbrites, which show log normal distribution with one mode each. The mean NRM value of the overall basalt population is 5.5 A/m +0.7/−0.6; this value is similar from that found by Prévot and Grommé (1975) for continental and sub-aerial basalt. The ignimbrite on the other hand has mean 0.22 A/m +0.4/−0.3. The standard deviation of the mean of the NRM for ignimbrite is large and the mean with the uncertainty overlaps the bimodal NRM intensity means reported earlier (Kidane et al., 2006).

The paleomagneic direction results from both the basalts and ignimbrites are simple and show clearly defined orthogonal vector component diagrams (Fig. 4).

3.3. Paleomagnetic directions

Careful partial demagnetization revealed two components of NRM. The low stability component mostly has been removed by imposing an alternating field of 10–15 mT or by heating above a temperature of 250 °C; the high stability component represents the Characteristic Remanent Magnetization (ChRM). Fig. 4(a–c) give representative Zijderveld diagrams by basalt; ignimbrite and trachytic units of twin specimens treated by both AF and TH techniques from normal and reversed polarities. The direction of the ChRM component or the principal component analysis are determined by using the best-fitting line of least square technique passing through the origin (Kirschvink, 1980). The maximum angular deviation (MAD) for most of the ChRM is less than 1° and no specimens had MAD > 4°. A few specimens from some sites did not have stable end points and linear segments could not be isolated. Where there were partial overlaps of more than one component, the technique of remagnetization circles has been used (Halls, 1976, 1978).

The ChRM identified by AF and TH techniques are identical with quasi-single magnetization (Fig. 4). The ChRM components determined at specimen level then were used to calculate the sample and site (flow) averages using Fisher (1953) statistics or McFadden and McElhinny (1988) statistics for combined analysis of remagnetization circles and stable linear segments. The paleomagnetic data analysis from principal component determination to calculation of overall mean direction was done using the paleomac software (Cogné, 2003).

3.3.1. Mean directions

The site mean ChRM directions are reported in Table 1. Sites are numbered from FT01 to FT28, the site-mean ChRM of sixteen sites are normal and ten sites are reversed while two sites are removed from the site mean ChRM direction (FT18 and FT27, anomalous directions). The compositions of the rocks at FT18 and FT27 are trachytic and basaltic respectively. The mean NRM intensities of the analyzed specimens from these sites do not show any marked

Table 1
Paleomagnetic site mean ChRM directions for all the analyzed rocks are reported here.

Sample name	Strike/Dip	Coordinates		N	D_g	I_g	D_s	I_s	K_s	α_{95}
		Latitude (°)	Longitude (°)							
FT01	0	8.91	39.87	6	348.8	20.2	348.8	20.2	435.3	3.3
FT02	0	9.02	39.85	6	350.8	21.1	350.8	21.1	646	2.6
FT03	0	9	39.82	6	350.7	2.7	350.7	2.7	127.1	6.7
FT04	015/15E	9	39.82	6	**159.3**	**−20.2**	165.0	−28.3	946.2	2.2
FT05	0	9	39.82	6	163.9	−28.2	163.9	−28.2	58.1	9.9
FT06	0	9	39.82	6	174	−20.1	174	−20.1	363.3	3.5
FT07	017/20E	8.92	39.88	6	**350.7**	**15.0**	356.8	22.7	267	3.9
FT08	0	8.92	39.88	6	0.8	14	0.8	14	359.9	3.5
FT09	0	8.95	39.91	6	0.4	6.6	0.4	6.6	31.4	12.1
FT10	0	8.95	39.91	6	350.7	20.2	350.7	20.2	1433.1	1.8
FT11	0	8.89	39.92	6	351.1	21.8	351.1	21.8	2268.7	1.4
FT12	0	8.86	39.9	6	355.1	4.7	355.1	4.7	127.5	7.1
FT13	0	8.85	39.89	6	2.3	20.2	2.3	20.2	213.4	4.8
FT14	0	8.89	39.92	6	351.2	22.2	351.2	22.2	454.8	3.1
FT15	210/21W	9.07	39.88	6	**165.2**	**−21.6**	161.6	−6.3	1899.3	1.5
FT16	0	9.04	39.86	6	350.7	22	350.7	22	473.1	3.1
FT17	184/17W	8.93	39.95	6	**352.5**	**19.1**	347.4	15	803.7	2.4
FT18	*0*	*8.93*	*39.95*	*6*	*301.5*	*43.5*	*301.5*	*43.5*	*106.5*	*7*
FT19	267/18W	8.95	39.97	5	**353.7**	**13.9**	353.8	−4	55.4	11.8
FT20	214/14W	8.96	40.01	6	168.5	−47.7	**160.1**	**−37**	222.6	4.5
FT21	0	8.95	40	3	13.9	9.1	13.9	9.1	136.4	10.6
FT22	0	8.92	40.03	6	162.2	−39.4	162.2	−39.4	131.3	7
FT23	0	9.02	40.18	6	182.2	−25.1	182.2	−25.1	417.3	3.3
FT24	0	9.02	40.18	6	178.9	−19.8	178.9	−19.8	696.2	2.5
FT25	0	9.02	40.18	6	185	−29.5	185	−29.5	541.1	2.9
FT26	0	9.1	40.01	6	348	15.2	348	15.2	72.8	8.5
FT27	0	9.05	40.06	6	202.8	11.8	202.8	11.8	176.4	5.1
FT28	0	9.01	40.07	6	175.4	−35.9	175.4	−35.9	193.1	4.9
Fentale Mean (Except FT18)				27	354.3	19.3	354.3	19.3	33.0	4.9
Metehara All Mean (Except FT18)				51	354.7	16.3	354.7	16.3	28.0	3.8
BC03 (1.5 Ma)				32	1.0	16.4	1.0	16.4	105.6	2.3

Sample name; Strike/Dip; location coordinates (the latitude and longitude); N, number of samples; D_g and I_g, declination and inclination in geographic coordinates; D_s and I_s, declination and inclination in stratigraphic coordinates; K, Fisher precision parameter; α_{95}, 95% confidence interval. The overall mean directions calculated for the sites from Fentale Surroundings ($N = 27$) and for the overall ($N = 51$), including 24 sites from a separate magnetostratigraphy study at Kereyou Lodge section. The 1.5 Ma expected mean reference curve of the dipole geomagnetic field for the Fentale area from Besse and Courtillot (2003) is shown. Italics indicate the site considered anomalous directions.

reductions. The NRM intensity values, 2.21 A/m for the former and 3.12 A/m for the latter, we obtained agree with the expected average values for basalts/trachytes (see Fig. 3), as a result it is difficult to suggest that they represent transitional fields. However, we can see that the VGP of site FT18 has deviated more than 40° (considered cut off angle; Barbetti & McElhinny, 1976) from the geographic pole while FT27 lies with in the ranges of stable polarity. As a result, we decided to exclude FT18 and keep FT27 in the directional analyses assuming it is part of the secular variation of stable polarity. The confidence interval (α_{95}) is listed in Table 1, and for most of the site-mean ChRM is less than 6° (only three samples have intervals greater than 10°), showing that the ChRM directions within sites are reasonably well clustered. So, the paleomagnetic directions obtained from these fresh lavas and pyroclastic flows of differing ages are of good quality data and we could determine the paleomagnetic pole with confidence (Table 2).

Fig. 5a and b are stereographic projection plots of site-mean ChRM directions; Fig. 5a shows the spatial samples of Fentale volcano region alone (this study); while Fig. 5b shows all site mean directions in the area including the 24 sites from Kereyou Lodge section combined to give overall mean ChRM directions for which we determined the paleomagnetic pole for the rocks of the Fentale products.

The separate normal and reversed polarities for the 27 sites in this study are $D_s = 354.5°$, $I_s = 15.6°$, $N = 16$, $K = 77$, $\alpha_{95} = 4.2°$ and $D_s = 173.9°$, $I_s = -24.8°$, $N = 11$, $K = 19.6$, $\alpha_{95} = 10.6°$; and for the entire data set (51 sites) including the Kereyou Lodge (Table 3) respectively are $D_s = 354.5°$, $I_s = 13.6°$, $N = 21$, $K = 34.1$, $\alpha_{95} = 5.5°$ and $D_s = 174.9°$, $I_s = -18.2°$, $N = 30$, $K = 25.1$, $\alpha_{95} = 5.4°$. The two polarities in both cases are antipodal and pass the paleomagnetic stability reversal test (McFadden and McElhinny, 1990). The overall site mean ChRM direction for the Fentale area including the anomalous direction (FT18) is: $D_s = 353°$, $I_s = 20.3°$, $N = 28$, $K = 23.8$, $\alpha_{95} = 5.7°$, excluding the anomalous site we get: $D_s = 354.3°$, $I_s = 19.3°$, $N = 27$, $K = 33$, $\alpha_{95} = 4.9°$). The results from this study combined with the Kereyou Lodge section allow calculation of overall averages. The overall mean including all directions is: $D_s = 354°$, $I_s = 16.9°$, $N = 52$, $K = 23.5$, $\alpha_{95} = 4.2°$. Excluding FT18, the mean becomes: $D_s = 354.7°$, $I_s = 16.3°$, $N = 50$, $K = 28.0$, $\alpha_{95} = 3.8°$. In most cases, the sampled sites were laid down sub-horizontally except for six sites where we have made necessary measurements of and corrections for previous tilting and the results are given (see Table 1). These six sites are (FT04, FT07, FT15, FT17, FT19, and FT20) and, their strikes and dips are given in Table 1. The outcrops of the first five sites were found either along streams or quarry exposure suggesting emplacement on originally tilted topography while the last (FT20) was along a fault scarp suggesting deformation after emplacement. Therefore, we considered the declination and inclination values in the geographic coordinates for the former and the tilt corrected values for the latter. The 95% confidence interval of the overall mean for the 27 sites (five of which are considered in geographic coordinates and FT20 in stratigraphic coordinates) become $\alpha_{95} = 4.9°$; when the geographic coordinates is considered for site FT20; the (α_{95}) increased to 5.1°; if we consider stratigraphic coordinate for all the sites, (α_{95}) increases to 5.3°. Therefore, the site-mean directions get more clustered when the five tilted sites are in geographic coordinates and FT20 in tilt corrected coordinates.

Table 2
Site mean virtual geomagnetic poles (VGPs) for all the analyzed rocks are reported here.

Sample Name	Strike/Dip	Coordinates		*N*	ϕ_g	λ_g	ϕ_s	λ_s	α_{95}
		Latitude (°)	Longitude (°)						
FT01	0	8.91	39.87	6	318.5	78.9	318.5	78.9	3.4
FT02	0	9.02	39.85	6	322.3	80.7	322.3	80.7	2.8
FT03	0	9	39.82	6	270.7	78	270.7	78	6.7
FT04	015/15E	9	39.82	6	**135.4**	**−69.5**	153.8	−74.1	2.4
FT05	0	9	39.82	6	152.3	−73.2	152.3	−73.2	10.8
FT06	0	9	39.82	6	143.5	−84	143.5	−84	3.7
FT07	017/20E	8.92	39.88	6	**302.0**	**80.5**	353.4	85.7	4.1
FT08	0	8.92	39.88	6	195.9	88.1	195.9	88.1	3.6
FT09	0	8.95	39.91	6	216.3	84.4	216.3	84.4	12.2
FT10	0	8.95	39.91	6	320.1	80.7	320.1	80.7	1.9
FT11	0	8.89	39.92	6	326.0	80.9	326	80.9	1.5
FT12	0	8.86	39.9	6	256.8	81.8	256.8	81.8	7.1
FT13	0	8.85	39.89	6	96.3	87.2	96.3	87.2	5
FT14	0	8.89	39.92	6	327.5	81	327.5	81	3.3
FT15	210/21W	9.07	39.88	6	**139.4**	**−75.3**	113	−70.7	1.5
FT16	0	9.04	39.86	6	325.4	80.5	325.4	80.5	3.3
FT17	184/17W	8.93	39.95	6	**317.9**	**82.6**	305.1	77.5	2.4
FT18	*0*	*8.93*	*39.95*	*6*	334.4	32.2	334.4	32.2	8.7
FT19	267/18W	8.95	39.97	5	**294.1**	**83.5**	249.8	77.4	11.8
FT20	214/14W	8.96	40.01	6	193.0	−67.3	**163.8**	**−67.5**	5.3
FT21	0	8.95	40	3	146.5	75.5	146.5	75.5	10.7
FT22	0	8.92	40.03	6	170.3	−68.3	170.3	−68.3	8.3
FT23	0	9.02	40.18	6	247.8	−85.3	247.8	−85.3	3.5
FT24	0	9.02	40.18	6	179.1	−88.4	179.1	−88.4	2.7
FT25	0	9.02	40.18	6	255.5	−81.6	255.5	−81.6	3.2
FT26	0	9.1	40.01	6	304.5	78.1	304.5	78.1	8.7
FT27	*0*	*9.05*	*40.06*	*6*	342.9	−62.8	342.9	−62.8	5.1
FT28	0	9.01	40.07	6	198.2	−78.2	198.2	−78.2	5.7
Fentale Mean 1 (All Sites)				28	324.9	82.5	324.9	82.5	5.0
Fentale Mean 2 (Except FT18)				27	322.0	84.1	322.0	84.1	3.9
Metehara Area Mean 1 (All Sites)				52	309.9	84.0	309.9	84.0	3.3
Metehara Area Mean 2 (Except site FT18)				51	305.5	84.8	305.5	84.8	2.8
BC03 (1.5Ma)				32	159.0	88.9	159	88.9	2.3

Sample name; Strike/Dip; location coordinates (the latitude and longitude); *N*, number of samples; ϕ_g and λ_g, pole longitude and latitude in geographic coordinates; ϕ_s and λ_s pole longitude and latitude in stratigraphic coordinates; *K*, Fisher precision parameter; α_{95}, 95% confidence interval. The overall mean VGPs directions calculated for the Fentale Surroundings ($N = 28$ and $N = 27$) and for the overall ($N = 52$ and $N = 51$), including 24 sites from a separate magnetostratigraphy study at Kereyou Lodge section. The mean VGP from Aparent Polar Wander Path Curve of Besse and Courtillot (2003) is also given as BC03.

Table 3
Paleomagnetic site mean ChRM directions for all the sites of the Kereyou Lodge (latitude 8.9°; longitude 40.1°) are reported.

Sample Name	*N*	D_g	I_g	D_s	I_s	K_s	α_{95}
KL01	7	186.4	−31.5	186.4	−31.5	648.3	2.4
KL02	7	178.5	−23.3	178.5	−23.3	582.0	2.6
KL03	7	183.2	−22.6	183.2	−22.6	118.0	5.6
KL04	7	186.4	−25.4	186.4	−25.4	523.1	2.6
KL05	7	176.7	−19.7	176.7	−19.7	653.7	2.4
KL06	7	177.1	−27.1	177.1	−27.1	1419.1	1.6
KL07	7	178.3	−17.5	178.3	−17.5	593.1	2.5
KL08	7	182.6	−14.9	182.6	−14.9	505.6	2.7
KL09	7	180.7	−10.6	180.7	−10.6	345.6	3.3
KL10	7	181.5	−15.6	181.5	−15.6	505.1	2.7
KL11	7	180.1	−11.8	180.1	−11.8	516.8	2.7
KL12	7	179.4	−12.3	179.4	−12.3	1068.5	1.8
KL13	7	163.7	−9.8	163.7	−9.8	106.7	6.0
KL14	7	164.8	−3.0	164.8	−3.0	196.8	4.6
KL15	7	165.9	−0.8	165.9	−0.8	168.4	4.9
KL16	7	163.0	−3.0	163.0	−3.0	154.0	5.4
KL17	7	154.1	4.7	154.1	4.7	99.5	6.1
KL18	5	174.7	−29.8	174.7	−29.8	588.3	3.2
KL19	7	181.2	3.1	181.2	3.1	63.5	8.4
KL20	6	357.8	−33.5	357.8	−33.5	87.3	7.7
KL21	7	352.3	9.5	352.3	9.5	239.1	4.0
KL22	7	346.0	10.2	346.0	10.2	155.1	5.0
KL23	7	352.7	16.8	352.7	16.8	276	4.0
KL24	7	4.5	28.0	4.5	28.0	177	4.5
Kereyou Mean1 (All Sites)	24	355.3	12.9	355.3	12.9	25.1	6.0
BC03 (1.5Ma)	32	1.0	16.4	1.0	16.4	105.6	2.3

Sample name; *N*, number of samples; D_g and I_g, declination and inclination in geographic coordinates; D_s and I_s, declination and inclination in stratigraphic coordinates; *K*, Fisher precision parameter; α_{95}, 95% confidence interval. The overall mean direction for ($N = 24$) is also given. The 1.5 Ma expected mean reference curve of the dipole geomagnetic field for the Fentale area from Besse and Courtillot, 2003 is shown.

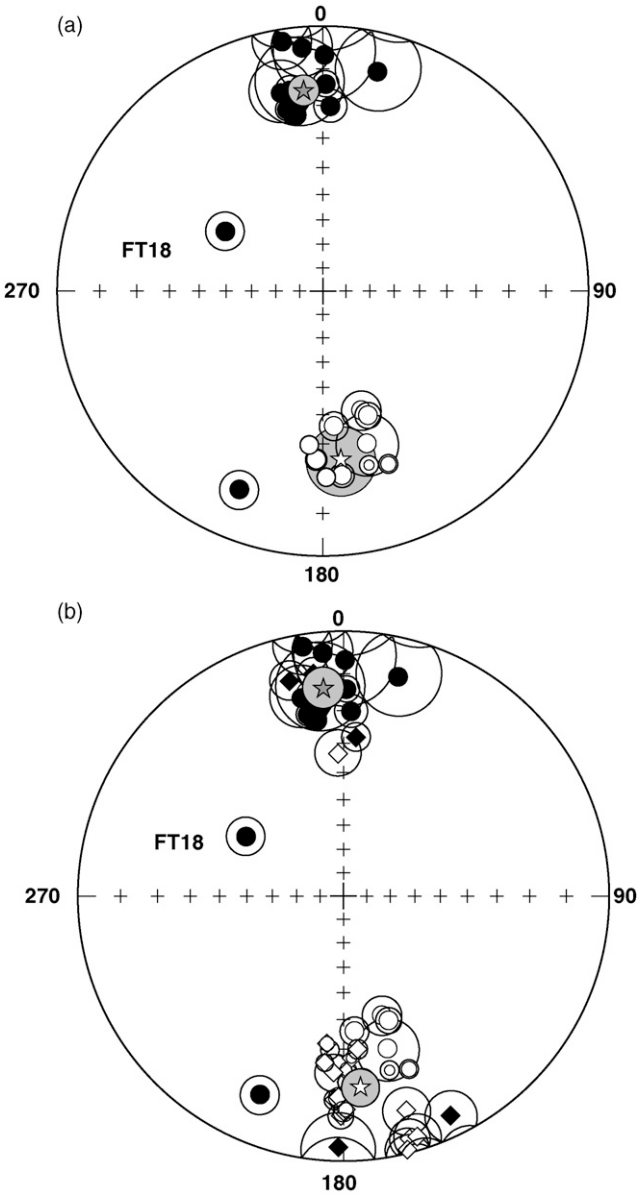

Fig. 5. Stereogram of the site mean ChRM (Characteristic Remanent Magnetization) directions with separate mean directions (shown with star symbols and confidence interval is shown with grey zone) calculated for normal and reversed polarities for the two groups described in the text. (a) Fentale surrounding, and (b) the database from Kereyou Lodge Magnetostratigraphic section (Table 3) and the current result combined. From all the diagrams the normal and reversed polarities are antipodal. One of the sites whose point is labeled as FT 18 has a direction extremely deviating from the rest of the directions. The directional value of this site is also given in Table 1.

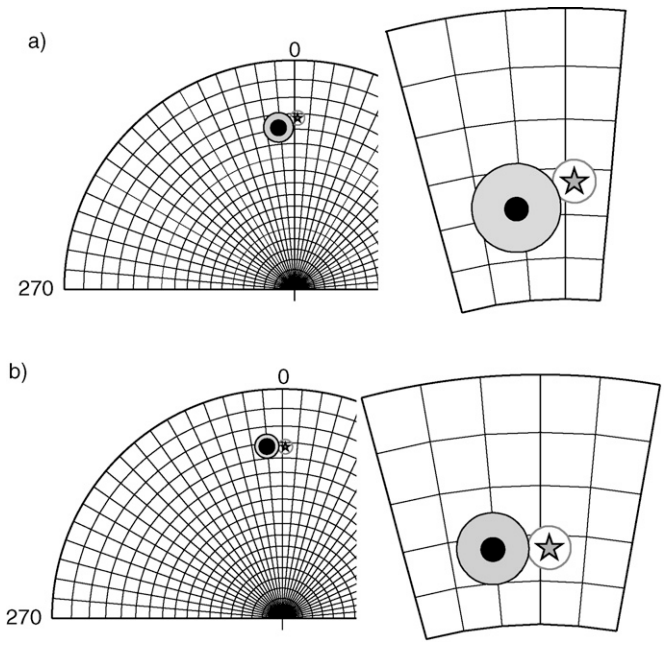

Fig. 6. Stereogram of the overall mean ChRM directions calculated after inverting the reversed polarities to their normal counterpart excluding the anomalous direction (FT18) for the two groups discussed above; (a) Fentale surrounding, and (b) the two combined. For all cases, in the blown up stereogram, the star symbol indicates the mean expected reference dipole geomagnetic field from (Besse and Courtillot, 1991; Besse and Courtillot, 2003) for the Fentale region and the full black circles with darker grey circles of 95% confidence interval is overall mean ChRM excluding the anomalous direction.

4. Discussions and interpretations

4.1. Tectonic rotations

The overall site mean directions for Fentale region and the overall mean combined from these directions were compared with the expected mean geomagnetic dipole reference field directions (Besse and Courtillot, 1991; Besse and Courtillot, 2003) for the Fentale co-ordinates assuming an average age of 1.5 Ma (i.e., $D = 1.0^\circ$, $I = 16.4^\circ$, $\alpha_{95} = 2.3^\circ$, $K = 105.6$, $N = 32$). The overall mean directions calculated for Fentale and the combined data for the region are given in Section 3.3.1, in Table 1 and also in Fig. 6.

The overall mean directions calculated by excluding the anomalous direction are used in all comparisons with the reference dipole field. For the Fentale surroundings, the declination and inclination differs respectively from the reference direction by $\Delta D = -6.7^\circ \pm 4.3^\circ$, $\Delta I = -2.9^\circ \pm 4.3^\circ$. When the 24 site mean directions at the Kereyou Lodge magnetostratigraphic section are included (database around Metehara region, which we will refer to as database in the next sections), these differences become: $\Delta D = -6.3^\circ \pm 4.4$, $\Delta I = 0.1^\circ \pm 4.4^\circ$.

The 95% confidence interval circle of the observed directions in both cases above and the confidence circle of the expected direction cut one another. Further comparison of these two mean directions McFadden and McElhinny (1990) vindicated that the directions are statistically different; hence both results indicate that tectonic block rotations about a vertical have occurred within the Fentale magmatic segment. The rotation about vertical axis is given by the difference in declinations, $R = -6.3^\circ \pm 4.4^\circ$; this value proves presence of a statistically significant counterclockwise rotation. The magnetostratigraphy at Kereyou Lodge section also recorded significant counterclockwise rotation (Kidane et al., GJI under review) and indicates that there is a systematic inclination change with age. This change is not observed on the calculated inclination difference with the dipole field ($F = 1.7^\circ \pm 5.7^\circ$), however, this result becomes more interesting when we see the systematic individual site mean inclination change down the section shown in Fig. 7, reversed polarity interval at the top became progressively shallow while normal polarity interval at the bottom became progressively steep, see Kidane et al. (GJI under review 2009) for details.

4.2. Virtual geomagnetic poles (VGP) & paleosecular variation (PSV)

The site mean VGP distributions are shown in Fig. 8 for both the Fentale surrounding and for the whole database including

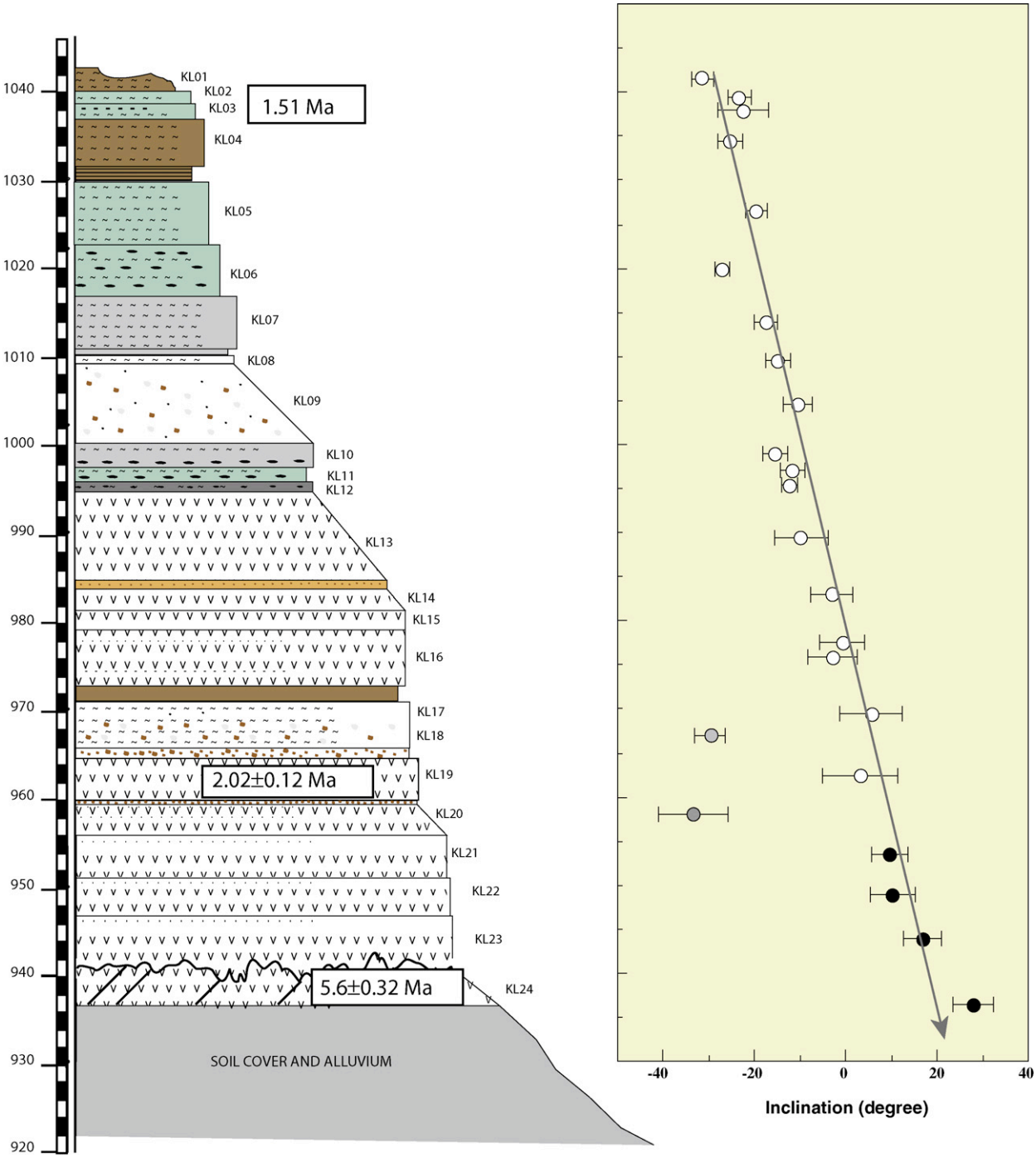

Fig. 7. Composite volcanic stratigraphy at the Kereyou Lodge section together with the paleomagnetic inclination result of the current results showing systematic and progressive inclination flattening from top to bottom of the section.

the database from Kereyou Lodge. The overall mean VGP value for the Fentale surrounding is $\phi = 324.9^\circ$, $\lambda = 82.5^\circ$, $K = 30.9$, $N = 28$, $A_{95} = 5.0^\circ$ and $S = 14.8^\circ$. This changes to $\phi = 322^\circ$, $\lambda = 84.1^\circ$, $K = 52$, $N = 27$, $A_{95} = 3.9^\circ$ and $S = 11.3^\circ$ when one anomalous site is excluded (Fig. 8a).

When the Fentale surrounding data is combined with the database for the Kereyou Lodge section an overall mean VGP of $\phi = 309.9^\circ$, $\lambda = 84.0^\circ$, $K = 37.3$, $N = 52$, $A_{95} = 3.3^\circ$ and $S = 13.5^\circ$, is obtained. This changes to $\phi = 305.5^\circ$, $\lambda = 84.8^\circ$, $K = 51.4$, $N = 51$, $A_{95} = 2.8^\circ$ and $S = 11.4^\circ$, when one anomalous site is excluded (Fig. 8b).

Since the Fentale magmatic segment has undergone tectonic rotation, the individual VGPs calculated are used to determine the VGP Scatter with respect to the mean directions. Separate VGP scatters were calculated for the two groups: Fentale region, and the combination of the two (Metehara region). So, for the for-

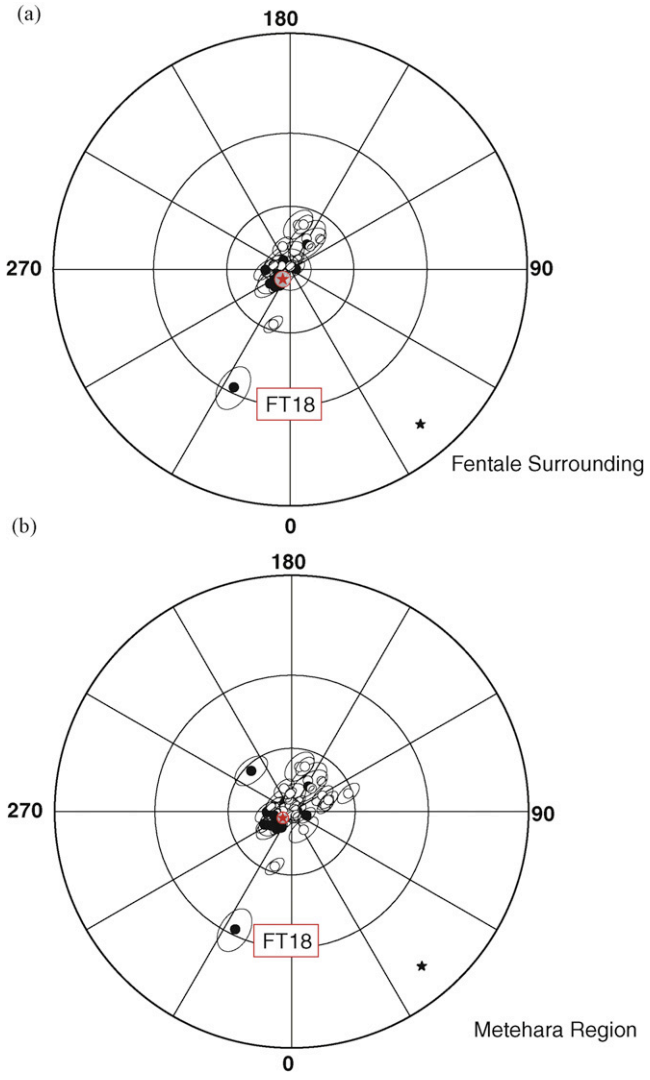

Fig. 8. Stereogram of the site mean VGP (Virtual Geomagnetic Pole) directions with separate mean directions (shown with full red colored star symbols with red colored confidence interval circle and light grey background) calculated for both polarities for the two groups described in the text is given. (a) Fentale surrounding, and (b) the two combined. From all the diagrams the site with anomalous direction (with VGP close smaller than 40°, FT 18) is labeled. The value of this data is also given in Table 2.

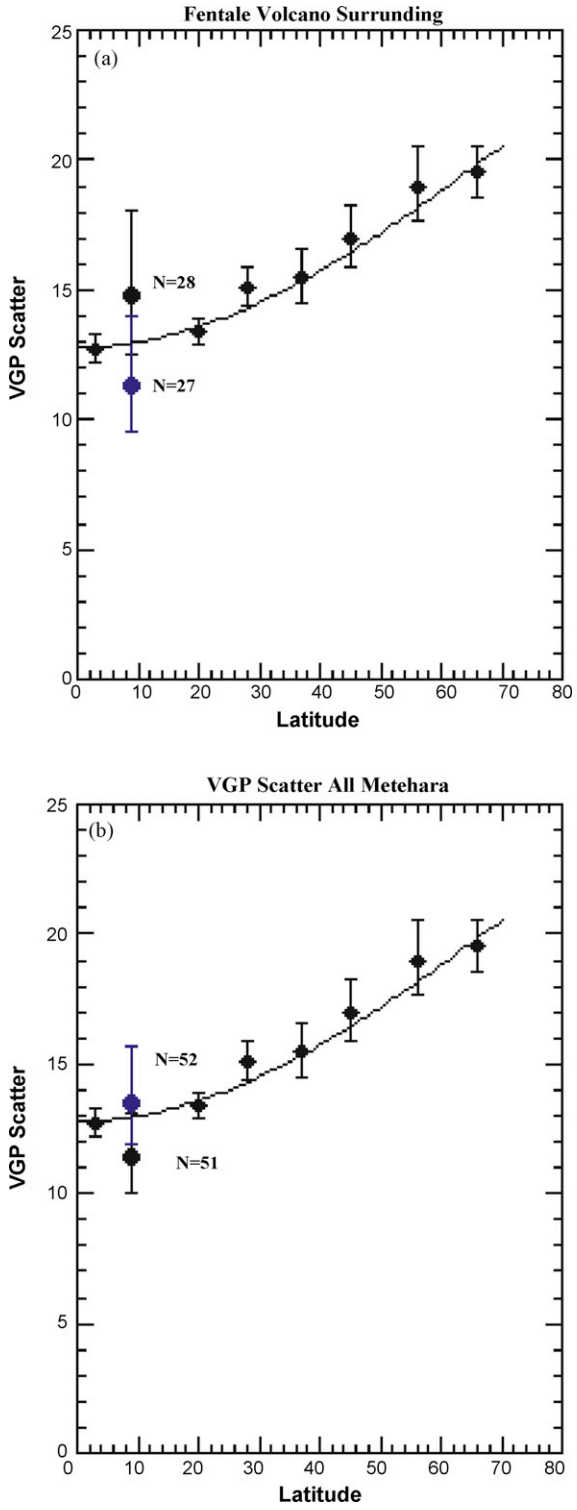

Fig. 9. Comparison of observed VGP scatter calculated using the Paleomac software (Cogné, 2003) for the rocks of the Fentale magmatic segments, MER, for the two groups described in the text. (a) Fentale surroundings (for $N = 27$ and $N = 28$), and (b) the two combined (for $N = 51$ and $N = 52$) with the reference curve of McFadden et al. (1991) for the period between 0 and 5 Ma.

mer two VGP Scatter were calculated, when all sites are included, VGP Scatter is 14.8° (confidence interval 12.5–18.1°), when one site is excluded the VGP Scatter changes to 11.3° (confidence interval 9.5–14.0°) (Cox, 1969; Cogné, 2003). For the combined data, when all sites are used the VGP Scatter is 13.5° (confidence interval 11.9–15.7°), when one site is excluded VGP Scatter reduces to 11.4° (confidence interval 10.0–13.1°). Because the age ranges of the studied lava flows is between 2.2 Ma and 1 Ma and both reversed and normal polarities are recorded in different locations, the VGP scatter should reflect the paleosecular variation of the geomagnetic field. Considering the uncertainties, the obtained VGP Scatter values are in good agreement with the recent 0–5 Ma model of McFadden et al. (1991). Fig. 9 shows comparison between the calculated VGP Scatter for the MER and the reference curve of McFadden et al. (1991) for the period between 0 and 5 Ma. The obtained result is in better agreement when all the data in the Metehara region (Fentale region and Kereyou Lodge section) are used indicating that they are part of the secular variation. When only those with stable directions are used, the mean VGP Scatter becomes somewhat smaller but it touches with the uncertainty the predicted value on the reference curve.

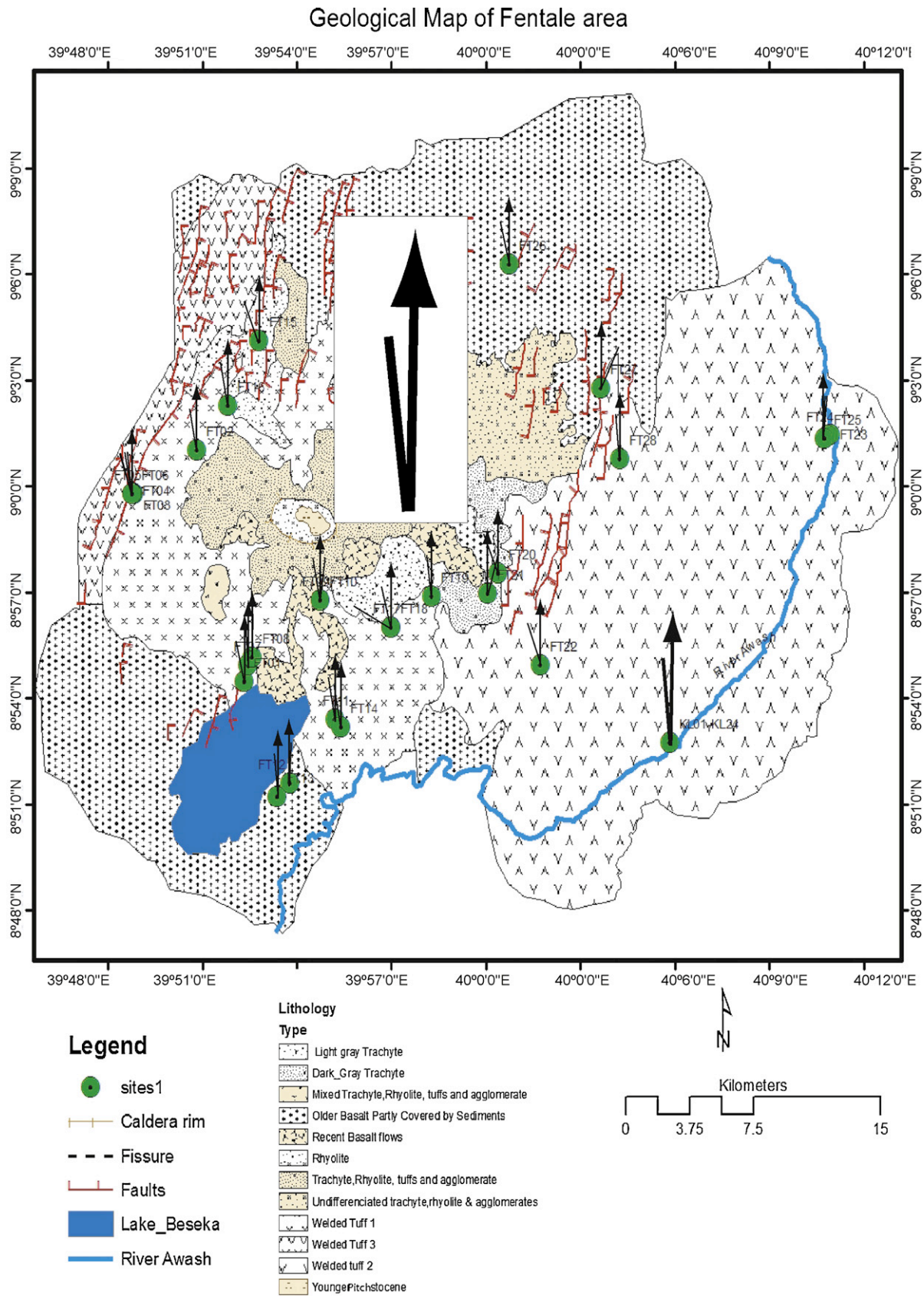

Fig. 10. Geological map of the study area shows the major lithologies that were sampled (modified from Williams et al., 2004), on which the site mean direction (as lines) and expected dipole positions (arrow) are given. The longer line arrow is for the mean direction along the Kereyou Lodge while the thick line and arrow in a white background stands for the overall mean direction.

5. Conclusions

The site mean ChRM directions are excellent directional data sets recorded from fresh unaltered volcanic rocks around Fentale Volcano. The ages of most rocks analyzed range in from 2.2 to 0.17 Ma, indicating significant time intervals are covered in this study. Various geological units in the above time interval were erupted from the volcanic centers of Fentale (Fig. 2). Geomagnetic polarity reversals have been recorded both along the magnetostratigraphic section of Kereyou Lodge and in sampling sites around Fentale. The VGP Scatter measured for the studied region, despite the small confidence limits and more clustered data sets, also indicates that secular variations have been well averaged out. The site mean paleomagnetic directions for all the sampled sites around Fentale are indicated in Fig. 10 as lines rotated from north (vertical), which is shown as a vertical arrow. The overall site mean directions calculated for Fentale region, and Metehara region, are indicated by relatively bigger arrows and all show consistent ~7° counterclockwise about vertical axis rotation in the Fentale magmatic segment. This result agrees well with the transtentional fault geometry inferred in this magmatic segment (Casey et al., 2006). In addition, the systematic inclination change along the Kereyou Lodge section possibly indicates rotations about horizontal axis due to rift-ward and margin-ward dipping beds whose amount increases progressively from top to bottom suggesting existence of deformation growth fault in the vicinity. These results indicate that like the along-strike variations in the geological, structural, and geophysical observations, block rotations also change along the strike of the Main Ethiopian Rift. Therefore, no single previous model of deformation could explain the mechanism of deformation in the entire MER; instead multiple styles and mechanisms of deformation characterize the upper crustal deformation mechanism in the MER. Hence, we recommend complete paleomagnetic mapping in the five magmatic segments, which could shed light on the regional deformation mechanisms prior to modeling.

Our observation of variations in along axis kinematics agrees with clay model experiments (Clifton et al., 2000) that show that rift obliquity is related to the acute angle, α, between the rift trend and displacement direction. The trend of the rift in the Fentale magmatic segment ranges from N10°E–N20°E (Casey et al., 2006 and Fig. 2), with Quaternary faults having mean orientation of N15°E and the Miocene border faults trending between N45°E and N50°E. Between the border faults and the magmatic segment, faults of two trends can be observed: N15°E and N45°E. In this region, rhomb shaped fault blocks have formed by the N45E-trending linkage of right stepping N15E rift-parallel faults, attesting to a dominance of transtensional deformation after 2 Ma. The recent displacement direction or opening direction from various independent studies is estimated to be between 105° and 110° (Keir et al., 2006; Bilham et al., 1999; Calais et al., 2006; Pizzi et al., 2006), near perpendicular to the Quaternary faults and aligned volcanic centers (Keir et al., 2006). Therefore, for this opening direction the angle $\alpha = 90°$ and as a result, normal faults develop along the rift axis, in contrast, for the areas between the magmatic segment and rift margin the angle α, ranges from 55° to 65°. Which according to the Clifton et al. (2000) model, two sets of faults develop in the described regions in accordance with the observation that faults of two trends forming the rhomb shaped depressions in the Northwestern part of the study area. In other magmatic segments within the MER, the coexistence of the faults with two trends have not been observed, which could explain the absence of rotation in the Assela area compared to the counterclockwise rotation quantified by paleomagnetism in the Fentale area.

Acknowledgement

We would like to express our gratitude to the Research and Publication office of Addis Ababa University for funding part of this work. We are also indebted to Dr. Takemoto and Dr. Yokoyama for their help during sample measurement stages, in the paleomagnetic laboratory of Kobe University. The first author also appreciates JSPS for funding his long and short-term fellowship and grants. In addition the funding support from the Research and Publication Office of Addis Ababa University all contributed to the findings of this research. We are very thankful for Mark Jellinek, Mike Fuller and one anonymous reviewer for providing useful comments that improved our manuscript.

References

Abebe, B., 1993. Studio geologico-structurale del Rift Etiopico a sud di Assela. Ph.D. Thesis. University of Frienze, Florence, Italy, pp. 153.
Acoccella, V., Korme, T., 2002. Holocene extension direction along the Main Ethiopian Rift, East Africa. Terra Nova 14 (3), 191–197.
Acton, G.D., Tessema, A., Jackson, M., Bilham, R., 2000. The tectonic and geomagnetic significance of paleomagnetic observations from volcanic rocks from central Afar, Africa. Earth Planet. Sci. Lett. 180, 225–241.
Barbetti, M.F., McElhinny, M.W., 1976. The Lake Mungo geomagnetic excursion. Phil. Trans. R. Soc. A 281, 515.
Bastow, I., Stuart, G., Kendall, M., Ebinger, C., 2005. Upper mantle Seismic structure in a region of incipient continental break-up: northern Main Ethiopian Rift. Geophys. J. Int. 162, 479–493.
Benoit, M.H., Nyblade, A.A., Vandecar, J.C., Gurrola, H., 2003. Upper mantle P velocity structure and mantle transition zone thickness beneath the Arabian Shield. Geophys. Res. Lett. 30, 1153.
Besse, J., Courtillot, V., 1991. Revised and synthetic apparent polar wander paths of the African, Eurasian, North American and Indian plates, and true polar wander since 200 Ma. J. Geophys. Res. 96, 4029–4050.
Besse, J., Courtillot, V., 2003. Apparent and True Polar wander and the geometry of the geomagnetic field in the last 200 million years. J. Geophys. Res. 108 (B10), 2469, doi:10.1029/2003JB002684.
Bilham, R., Bendick, R., Larson, K., Mohr, P., Braun, J., Tesfaye, S., Asfaw, L., 1999. Secular and tidal strain across the Main Ethiopian Rift. Geophys. Res. Lett. 26, 2789–2792.
Boccaletti, M., Getaneh, A., Tortorici, L., 1992. The Main Ethiopian Rift: an example of oblique rifting. Ann. Tecton. 6, 20–25.
Boccaletti, M., Mammo, T., Bonini, M., Abebe, B., 1994. Seismotectonics of East African Rift System: evidence of active oblique rifting. Ann. Tecton. 8, 87–99.
Boccaletti, M., Bonini, M., Mazzuoli, R., Abebe, B., Piccardi, L., Tortorici, L., 1998. Quaternary oblique extensional tectonics in the Ethiopian Rift (Horn of Africa). Tectonophysics 287, 97–116.
Bonini, M., Souriot, T., Boccaletti, M., Brun, J.P., 1997. Successive orthogonal and oblique extension episodes in a rift zone: Laboratory experiments with application to the Ethiopian rift. Tectonics 16, 347–362.
Calais, E., Ebinger, C., Keir, D., Gloaguen, R., Mohammed, F., 2006. Strain accommodation in transitional rifts: Extension by magma intrusion and faulting in Ethiopian rift magmatic segments. In: Yirgu, G., Ebinger, C.J., Maguire, P.K.H. (Eds.), The Afar Volcanic Province within the East African Rift System, vol. 259. J. Geol. Soc., London, pp. 143–163.
Casey, M., Ebinger, C., Keir, D., Gloaguen, R., Mohammed, F., 2006. Strain accommodation in transitional rifts: extension by magma intrusion and faulting in Ethiopian rift magmatic segments. In: Yirgu, G., Ebinger, C.J., Maguire, P.K.H. (Eds.), The Afar Volcanic Province within the East African Rift System, vol. 259. J. Geol. Soc., London, pp. 143–163.
Chorowicz, J., Collet, B., Bonavia, F.F., Korme, T., 1994. Northwest to north-northwest extension direction in the Ethiopian Rift deduced from the orientation of extension structures and fault slip analysis. Geol. Soc. Am. Bull. 105, 1560–1570.
Clifton, A.E., Schlisch, R.W., Withjack, M.A., Ackermann, R.V., 2000. Influence of rift obliquity on fault–population systematics results of experimental clay models. J. Struc. Geol. 22, 1491–1509.
Cogné, J.P., 2003. Paleomac, a Macintosh application for treating paleomagnetic data and making plate reconstructions. Geochem. Geophys. Geosyst. 4 (1), 1007, doi:10.1029/2001GC000227.
Cox, A., 1969. Confidence limits for the precision parameter K. Geophys. J. R. Astron. Soc. 18, 545–549.
Di Paola, G.M., 1972. The Ethiopian Rift Valley (between 7° and 8°40′ lat North). Bull. Volcanol. 35, 497–506.
Ebinger, C., Yemane, T., Harding, D., Tesfaye, S., Rex, D., Kelley, S., 2000. Rift deflection, migration, and propagation: Linkage of the Ethiopian and Eastern rifts, Africa. Geol. Soc. Am. Bull. 102, 163–176.
Ebinger, C.J., Casey, M., 2001. Continental breakup in magmatic provinces: An Ethiopian example. Geology 29, 527–530.
Fisher, R.A., 1953. Dispersion on a sphere, Proc, Roy. Soc. London, A. 217, 295–305.
Halls, H.C., 1976. A least-squares method to find a remanence direction from converging remagnetization circles. Geophys. J. R. Astron. Soc. 45, 297–304.

Halls, H.C., 1978. The use of converging remagnetization circles in paleomagnetism. Phys. Earth Planet. Int. 16, 1–11.
Hofmann, C., Courtillot, V., Féraud, G., Rochette, P., Yirgu, G., Ketefo, E., Pik, R., 1997. Timing of the Ethiopian flood basalt event and implications for plume birth and global change. Nature 389, 838–841.
Keir, D., Ebinger, C., Stuart, G., Daly, E., Ayele, A., 2006. Strain accommodation by magmatism and faulting as rifting proceeds to breakup: Seismicity of the northern Ethiopian Rift. J. Geophys. Res. 111, B05314, doi:10.1029/2005JB003748.
Keranen, K., Klemperer, S., Gloaguen, R., Eagle Working group, 2004. Imaging a proto-ridge axis in the Main Ethiopian Rift. Geology 39, 949–952.
Kenea, N.H., Ebinger, C.J., Rex, D.C., 2001. Late Oligocene volcanism and extension in the southern Red Sea Hills Sudan. J. Geol. Soc. London 158, 285–294.
Kidane, T., Carlut, J., Courtillot, V., Gallet, Y., Quidelleur, X., Gillot, P.-Y., Haile, T., 1999. Paleomagnetic and geochronological identification of the Reunion subchron in Ethiopian Afar. J. Geophys. Res. 104 (B5), 10,405–10,419.
Kidane, T., Courtillot, V., Manighetti, I., Audin, L., Lahitte, P., Quidelleur, X., Gillot, P.-Y., Gallet, Y., Carlut, J., Haile, T., 2003. New paleomagnetic and geochronologic results from Ethiopian Afar: Block rotations linked to rift overlap and propagation and determination of a ~2 Ma reference pole for stable Africa. J. Geophys. Res. 108 (B2), 2102, doi:10.1029/2001JB000645.
Kidane, T., Platzman, E., Ebinger, C., Abebe, B., Rochette, P., 2006. Paleomagnetic constrains on continental break-up processes: Observations from the Main Ethiopian Rift. In: Yirgu, G., Ebinger, C.J., Maguire, P.K.H. (Eds.), The Afar Volcanic Province within the East African Rift System, vol. 259. J. Geol. Soc., London, pp. 165–183.
Kieffer, B., Arndt, N., Lapierre, H., Bastien, F., Bosch, D., Pecher, A., Yirgu, G., Ayalew, D., Weiss, D., Jerram, D.A., Keller, F., Meugniot, C., 2004. Flood and shield basalts from Ethiopia: Magmas from the African superswell. J. Petrol. 45, 793–834.
Kirschvink, J.L., 1980. The least squares line and plane and the analysis of paleomagnetic data. Geophys. J. R. Astron. Soc. 62, 699–718.
Korme, T., Chorowicz, J., Collet, B., Bonavia, F.F., 1997. Volcanic vents rooted on extension fractures and their geodynamic implications in the Ethiopian Rift. J. Volcanol. Geotherm. Res. 79, 205–222.
Mahatsente, R., Jentzsch, G., Jahr, T., 1999. Crustal structure of the Main Ethiopian Rift from gravity data: 3-dimensional modeling. Tectonophysics 313 (4), 363–382.
McFadden, P.L., McElhinny, M.W., 1990. Classification of the reversal test in paleomagnetism. Geophys. J. Int. 103, 725–729.
McFadden, P., Merrill, L., McElhinny, M.W., Lee, M.W.S., 1991. Reversals of the Earth's magnetic field and temporal variations of the dynamo families. J. Geophys. Res. 96, 3923–3933.
McFadden, P.L., McElhinny, M.W., 1988. The combined analysis of remagnetization circles and direct observations in paleomagnetism. Earth Planet. Sci. Lett. 87, 152–160.
Meyer, W., Pilger, A., Rosler, A., Stets, J., 1975. Tectonic evolution of the northern part of the Main Ethiopian Rift in Southern Ethiopian, "Afar depression of Ethiopia", in: A. Pilger, A. Rosler (eds.), IUGG Sci. Rep., Stuttgart, 14, pp. 352–362.
Mohr, P.A., 1962. The Ethiopian Rift System. Bull. Geophys. Obs. Addis Ababa Univ., 5, pp. 33-62.
Pik, R., Marty, B., Carignan, J., Lave, J., 2003. Stability of the Upper Nile drainage network (Ethiopia) deduced from (U-Th)/He thermochronometry: Implications for uplift and erosion of the Afar plume dome. Earth Planetary Sci. Lett. 215, 73–88.
Pizzi, A., Coltorti, M., Abebe, B., Disperati, L., Sacchi, G., Salvini, R., 2006. The Wnji fault belt (Main Ethiopian Rift): Structural and Geomorphological Constraints and GPS Monitoring. In: Yirgu, G., Ebinger, C.J., Maguire, P.K.H. (Eds.), The Afar Volcanic Province within the East African Rift System, vol. 259. J. Geol. Soc. London, pp. 191–207.
Prévot, M., Grommé, S., 1975. Intensity of magnetization of subaerial and sub-marine basalts and its possible change with time. Geophys. J. R. Astr. Soc. 40, 207–224.
Woldegabriel, G., Aronson, J.L., Walter, R.C., 1990. Geology, geochronology and rift basin development in the central sector of the Main Ethiopian Rift. Bull. Geol. Soc. Am. 102, 439–458.
Wolfenden, E., Ebinger, C., Yirgu, G., Renne, P., Kelley, S.P., 2005. Evolution of the southern Red Sea rift: Birth of a magmatic margin. Bull. Geolog. Soc. Am. 117, 846–864.
Williams, F.M., Williams, M.A.J., Aumento, F., 2004. Tensional fissures and crustal extension rates in the northern part of the Main Ethiopian Rift. J. African Earth Sci. 38, 183–197.